



Rapid Phase Transitions of Thermotropic Glycolipid Quasicrystal and Frank-Kasper Mesophases: A Mechanistic Rosetta Stone

Charlotte M. Wentz⁺, Kätchen K. Lachmayr⁺, Esther H. R. Tsai, and Lawrence R. Sita*

Abstract: Experimental results are presented that serve to lower the barrier for developing the science and technology of non-classical thermotropic glycolipid mesophases, which now include dodecagonal quasicrystal (DDQC) and Frank-Kasper (FK) A15 and σ mesophases that can be produced under mild conditions from a versatile class of sugar-polyolefin conjugates. By employing “alloys” comprised of mono- and disaccharide-polyolefin conjugates, and optionally with vitamin E as a small molecule phase modulator, we report the spontaneous formation of stable A15 mesophases at ambient temperature. We further document a rich thermotropic phase map that includes DDQC, A15, and σ mesophases of tunable periodicity that are connected through rapid thermotropic phase transitions as a function of increasing temperature in the order: liquid-like packing (LLP) \rightarrow DDQC \rightarrow A15 \rightarrow σ \rightarrow disorder. This first direct observation of a rapid thermotropic A15 \rightarrow σ phase transition provides support for a diffusionless martensitic process proceeding through strain-induced introduction of planar defects into the A15 lattice.

Introduction

Delineating the rules that dictate the design and rapid fabrication of soft matter quasicrystals (QC) and Frank-Kasper (FK) mesophases can have far-reaching implications for life, science, and technology.^[1] These range from questions regarding the abiotic origins of protocells with nascent capabilities for complex hierarchical compartmentalization of function,^[2] to the development of reconfigura-

ble smart materials for shape-shifting photonic applications.^[3] For these goals and others to become fully realized, however, new paradigms are required that can greatly accelerate the rate at which new structural categories of soft matter QC and FK phases are conceived and validated, and viable mechanisms for kinetically fast phase transitions that occur in the bulk under technologically-useful conditions are identified and exploited to provide thermodynamically-stable or long-term metastable states.

Soft matter FK mesophases can be viewed as arising through the tetrahedral-close-packing (TCP) of deformable micelle particles that must be able to accommodate the space-filling requirements of different distorted polyhedra that represent the Wigner-Seitz (WS) cells associated with unique sets of crystallographically distinct sites within the periodic lattice.^[1,4] As a corollary, since only a fixed number of these polyhedra can satisfy the requirements of TCP, and which are limited to those with the number of faces (Z) being 12, 14, 15, or 16, only a finite number of FK mesophases can exist. Figure 1 presents the packing arrangement of WS polyhedra associated with the unit cells for the FK A15 and σ phases, which are the two most commonly encountered for a wide structural range of soft matter.^[5–13] In cubic A15 ($Pm\bar{3}n$), a set of two equivalent corner-shared and body-centered sites are occupied by Z12 polyhedra (blue, Wyckoff position 2a) and these are complimented by another set of six equivalent face-shared sites that are filled by Z14 polyhedra (green, 6c), for a total of eight particles (see Figure 1b). The tetragonal σ ($P4_2/mnm$) phase is more complex in that five sets of unique sites now exist, and these are occupied by two Z12 (blue, 2b), eight Z12 (magenta, 8i), eight Z14 (green, 8i'), eight Z14 (red, 8j), and four Z15 (yellow, 4f) WS polyhedra for a total of thirty particles. In contrast, the much simpler classical body centered cubic (BCC) ($Im\bar{3}m$) unit cell consists of only a single set of two particles as shown in Figure 1b. Importantly, although slightly different shapes and cell volumes are associated with the various site-specific WS polyhedra (see Figure 1a), there is no *a priori* requirement that deformable micelles located at these different unit cell positions must be size differentiated with respect to the average aggregation number of micelle components, $\langle N \rangle$, if one is considering the full scope of kinetically trapped, metastable, and equilibrium-favoured mesophases within a particular system. Finally, the 3D lattices of the FK A15 and σ mesophases can be represented by 2D tiling schemes in which squares and triangles arise from the overlay of alternating layers with a “dense” ($z=0, \frac{1}{2}$ and 1) and “sparse” ($z=\frac{1}{4}$ and $\frac{3}{4}$) number of sites, with z being the lattice direction that is

[*] C. M. Wentz,⁺ K. K. Lachmayr,⁺ Prof. Dr. L. R. Sita
 Department of Chemistry and Biochemistry, University of Maryland
 College Park, MD 20742 (USA)
 E-mail: lsita@umd.edu

Dr. E. H. R. Tsai
 Center for Functional Nanomaterials, Brookhaven National Laboratory
 Upton, NY 11973 (USA)

[⁺] These authors contributed equally to this work.

© 2023 The Authors. Angewandte Chemie International Edition published by Wiley-VCH GmbH. This is an open access article under the terms of the Creative Commons Attribution Non-Commercial NoDerivs License, which permits use and distribution in any medium, provided the original work is properly cited, the use is non-commercial and no modifications or adaptations are made.

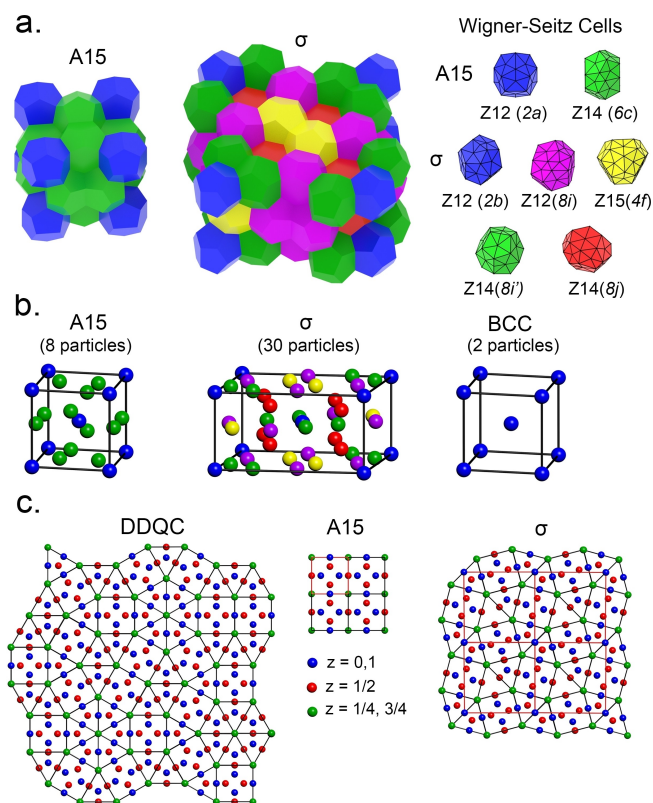


Figure 1. Schematic representations of (a) packing of WS polyhedra for unit cells of A15 and σ and color-coded with respect to the different sets of crystallographically unique sites at the Wyckoff positions shown in parentheses, (b) unit cells of A15, σ and BCC showing sets of equivalent crystallographic sites color-coded using spheres of equal but arbitrary size, and (c) 2D tiling patterns for DDQC, A15, and σ lattices with dense ($z=0, 1$) and sparse ($z=1/4, 3/4$) layers indicated by different color-coded spheres and with unit cells marked by red boundaries.

perpendicular to the plane of the tiling.^[5] The connection of A15 and σ mesophases to that of a soft matter DDQC now becomes apparent when one compares the 2D tiling representation for all three as presented in Figure 1c. Indeed, both A15 and σ are considered approximants for DDQC with the distinction that while the latter is aperiodic within the xy plane, it is still periodic in the z direction.

Over the past two decades, thermotropic QC and FK mesophases (e.g. A15, σ , C14 and C15 laves, and Z) have been discovered and characterized for several different classes of soft matter that include: dendritic liquid crystals (LCs), block copolymers, geometry-constrained “giant” molecules, and DNA and colloidal nanoparticles.^[6–14] Surprisingly, however, the relative stabilities and the mechanisms by which phase transitions can occur between various non-classical TCP and classical thermotropic mesophases still remain somewhat murky and unsettled. More to the point, there is increasing experimental agreement between results obtained for different soft matter categories that, within a given “one-component” system, the temperatures at which various classical and non-classical thermotropic mesophases appear is in the order: DDQC (lowest) < A15 <

σ < BCC (highest). However, establishing which of these observed mesophases represent kinetically trapped, metastable, or thermodynamic equilibrium states remains an unfulfilled goal that is complicated by the well-documented dramatic impact that small variations in the structures of very closely related micelle components can have on the thermotropic phase maps of many different types of soft matter. Regarding the mechanisms by which these thermotropic phase transitions occur, it has been proposed by many, and now almost universally accepted as dogma, that a reconstructive (*diffusion*) mechanism must be involved that results in changes to $\langle N \rangle$ and micelle size dispersity through intermicellar mass transfer of components. For instance, Bates, Lodge, and co-workers^[9] have proposed for a reversible thermotropic $\sigma \leftrightarrow$ BCC phase transition that a reconstructive process occurs through a repartitioning of $\langle N \rangle$ into different mesophase-dependent cardinal numbered sets of size-differentiated micelle particles that come about through mass transfer of components and micelle size self-sorting. On the one hand, a reconstructive phase transition mechanism would appear to be supported by the slow kinetics often reported for establishment of a new thermodynamically favoured soft matter TCP equilibrium mesophase, which requires several hours to days to even several months after a change in temperature has occurred. Further, while thermotropic A15 and σ mesophases have been observed to independently emerge for a one-component system at different temperatures, to date, there has not been a report of the direct observation of a A15 \rightarrow σ (or vice-versa) *order-order* phase transition. Looking at the change in complexity of the unit cells for each mesophase (see Figure 1b), one might instinctively assume that only a reconstructive mechanism is possible for interconversion of these two TCP lattices. On the other hand, group theory considerations establish that a symmetry-allowed cubic (A15) to σ (tetragonal) martensitic *diffusionless* pathway can potentially exist. And if validated, one would expect to be able to observe phase transition kinetics that are orders of magnitude faster than a reconstructive process, which then also opens the door to a much greater range of scientific questions and potential technological applications.

In 2019, we reported the first definitive example of a cyclic-hexose-based glycolipid thermotropic A15 mesophase for the sugar-polyolefin conjugate **1a** shown in Figure 2 that is comprised of a cellobiose (CB) disaccharide head group tethered to an atactic poly(4-methyl-1-pentene) (aPMP) tail through a 1,2,3-triazole linker that is formed via “click” chemistry between the two domain precursors.^[15] We further proposed a symmetry-allowed hexagonal-to-rhombohedral-to-cubic diffusionless phase transition mechanism that could account for results obtained from a variable temperature synchrotron small angle x-ray scattering (VT-SAXS) investigation in which an initial classical hexagonal cylindrical (H_c) mesophase was observed to rapidly convert into a final equilibrium A15 lattice through small in-plane positional displacements of micelle particles, followed by corona reshaping of the polyolefin domain to fulfil the space requirements of the WS polyhedra.^[15c] Importantly, in contrast to all other soft-matter TCP-based mesophases, this

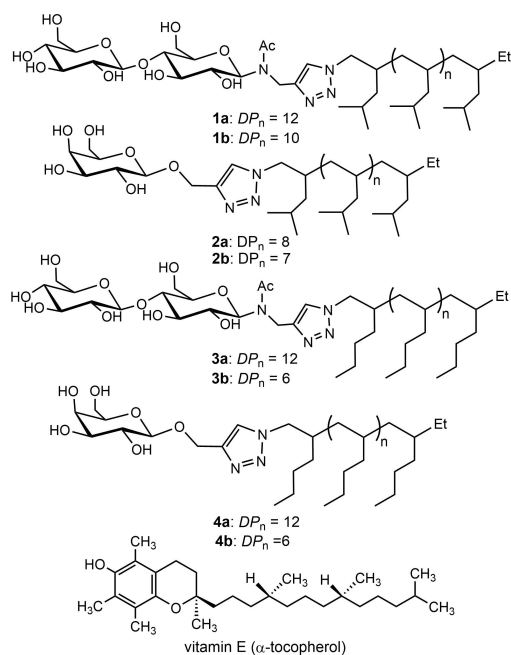


Figure 2. (a) Structures of mono- and disaccharide sugar-polyolefin conjugates **1–4** and vitamin E, Ac = acetyl.

final A15 mesophase of **1a** was shown to be exceedingly stable and robust under ambient conditions for periods of at least several months. Finally, within the same year, we quickly followed up these preliminary results with a report of the observation of more complex thermotropic phase behaviour of blends comprised of the CP-aPMP derivative **1b** and vitamin E in which the latter could be used as a “small molecule phase modulator” for globally lowering overall phase transition temperatures and providing access to not only A15, but σ and BCC mesophases of this sugar-polyolefin conjugate as well.^[15d] Figure 3 presents a summary of the important results obtained through a VT-SAXS study of these blends in which a triple point for co-existence of all three mesophases, {A15, σ , and BCC}, was established for different combinations of temperature and percent vitamin E within the blend with **1b**. An evaluation of the complete

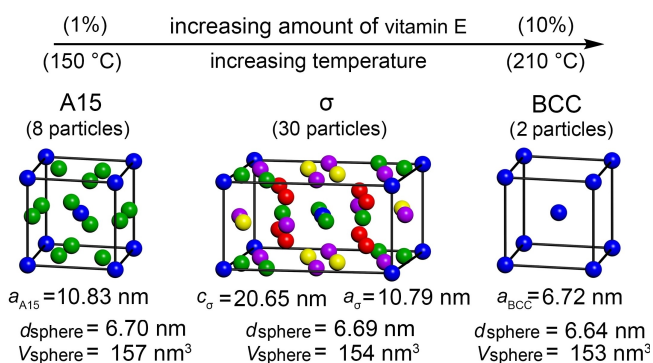


Figure 3. Thermotropic phase modulation of the mesophases of the cellobiose-aPMP sugar-polyolefin conjugate **1b** using temperature and blends with vitamin E.^[15d]

collection of VT-SAXS data led us to posit a relative stability ordering of A15 (most stable) < σ < BCC (least stable). Further, given the close similarity in the first-order-derived micelle dimensions presented in Figure 3, we speculated that these co-existing mesophases could possibly be interconverting through other cubic-to-tetragonal-to-cubic symmetry-allowed pathways involving small micelle particle displacements, rather than through a reconstructive process requiring repartitioning of $\langle N \rangle$ through intermolecular mass transfer and size-self-sorting. Unfortunately, this investigation did not establish conditions and blend compositions that could provide a pure glycolipid σ mesophase, nor were we able to capture evidence for a direct A15 \rightarrow σ order-order phase transition under either isothermal conditions or a temperature ramp within a synchrotron VT-SAXS study.

Herein, we now report new results obtained from our ongoing investigations of the thermotropic phase behaviour and mesophase structures of sugar-polyolefin conjugates in which the following advances are established: (1) the first example of a glycolipid A15 mesophase that spontaneously forms at ambient temperature, (2) the first examples of pure glycolipid DDQC and σ mesophases, (3) direct observation of a continuous series of rapid phase transitions within a sugar-polyolefin “alloy” blend that proceeds according to liquid-like packing (LLP) \rightarrow DDQC \rightarrow A15 \rightarrow σ \rightarrow disorder (DIS) as a function of increasing temperature, and (4) direct observation of a rapid A15 \rightarrow σ order-order phase transition that provides support for a symmetry-allowed diffusionless martensitic process that proceeds through simple strain-induced introduction of planar defects into the initial A15 lattice to directly provide the final σ mesophase. Collectively, these findings serve to significantly lower the barrier for development of the science and technology of non-classical glycolipid mesophases. Further, by extension, our discovery of thermotropic QC and FK mesophases of glycolipids that form under relatively mild conditions now raises the intriguing possibility and encourages the search for naturally occurring analogues that might exist within terrestrial and non-terrestrial environments.

Results and Discussion

The present project was motivated by the desire to answer the following questions: (1) can new designs for sugar-polyolefin conjugates be conceived and validated, and possibly as blends with vitamin E, to provide access to new TCP-based mesophases at, or near, ambient temperature? (2) can a pure σ mesophase be obtained, and if so, can it engage in verifiable order-order phase transitions with other thermotropic QC and FK mesophases? (3) can new insights be obtained regarding the enthalpic and entropic factors that dictate the relative stabilities of these TCP-based mesophases and provide the driving force for thermally mediated phase transitions? and (4) can new experimental data be acquired that shed light on the mechanisms by which rapid thermotropic phase transitions for sugar-polyolefin conjugates, and more expansively for all soft matter TCP-

based mesophases, can occur, and ideally, for the crypto-quintessential example of an A15 $\rightarrow\sigma$ order-to-order phase transition?

To address the first goal of forming TCP-based mesophases of sugar-polyolefin conjugates under near ambient conditions, a new design for the polyolefin domain was considered. For this purpose, the basic “first-order” design principals presented by Percec, Ungar, and co-workers in their seminal reports of the discovery and subsequent development of dendritic liquid crystal QC and FK mesophases was implemented.^[6] More specifically, these investigators have proposed using a 2D profile map of the self-organizing amphiphile to target new hydrophobic domain structures that have increased lateral extension vs longitudinal length that can then favour spherical inverse micelle formation and TCP packing. The question then becomes, how can one design and secure practical quantities of new *non-dendritic* hydrophobic domain building blocks that meet this criterion? In this regard, Hashim and co-workers^[16] have previously reported the thermotropic phase behaviour of glycolipids comprised of disaccharide “head” groups that are tethered to bifurcated long-chain “Guerbet” hydrocarbon “tails”, but no evidence of either QC or FK mesophases were reported. Further, in the foundational studies by Willson, Borsali, Isono and their respective co-workers,^[17] a variety of different polysaccharide-based block and graft copolymers were investigated, but only classical thermotropic mesophases, including lamellar (*L*), hexagonal cylindrical (*H_c*), and double gyroid (*DG*), have so far been observed.^[18,19]

We attribute the success of sugar-polyolefin conjugates to rapidly form both classical and non-classical thermotropic mesophases to the unique features of the polyolefin domain, which includes both ultra-low molar mass and a very narrow molar mass distribution (*cf.* $M_n=1.0$ kDa, $DP_n=12$, and $\bar{D} (=M_w/M_n)=1.03$ in **1a**) that serves to reduce chain entanglements and thereby allow for phase transitions to occur at greatly reduced temperatures than traditionally observed.^[15–19] As previously presented by us, a low-level molecular mechanics evaluation of **1a** further revealed that, at ambient temperature, the conformational space occupied by the aPMP is “wedge-shaped”, which favours initial formation of the columnar *H_c* morphology. However, at higher temperatures, the increased dynamics of this hydrophobic domain causes it to assume a more “conical-shape”, which then favors formation of spherical inverse micelles. The role played by the small molecule phase modulator vitamin E can be seen as similarly providing an increase in conformational occupied space through preferential sequestration and swelling of the polyolefin domain. Finally, one must also consider the balance of enthalpic and entropic factors that are associated with the size of the sugar domain (e.g. mono- vs. di- vs. polysaccharide), which undoubtedly includes a degree of hydrogen bonding between the domains within the aggregated core of the micelles. In this regard, we have previously reported that when a monosaccharide galactose (GAL) head group is tethered to an atactic polypropylene (aPP) domain tail ($DP_n=10$), a thermotropic *H_c* mesophase was obtained after thermal annealing at

60°C. In contrast, coupling of a GAL domain with a short aPMP tail ($DP_n=8$), as presented by **2** of Figure 2, now produced a “spherical” mesophase after thermal annealing at the same temperature as revealed by phase-sensitive tapping mode atomic force microscopy (ps-tm AFM).^[15a] Before discussing our new VT-SAXS structural studies with **2a** (see below), we hypothesized for the present study that an atactic poly(1-hexene) (aPH) domain might be able to fulfil the desired lateral vs. longitudinal design criterion for accessing thermotropic spherical inverse micelles at much lower temperatures. However, since it was not possible to predict *a priori* what the optimum relative domain sizes should be, we decided to initially target the pairing of both di- and monosaccharide head groups with new polyolefin tails of different DP_n values as presented by the sugar-polyolefin conjugates **3** and **4** in Figure 2.

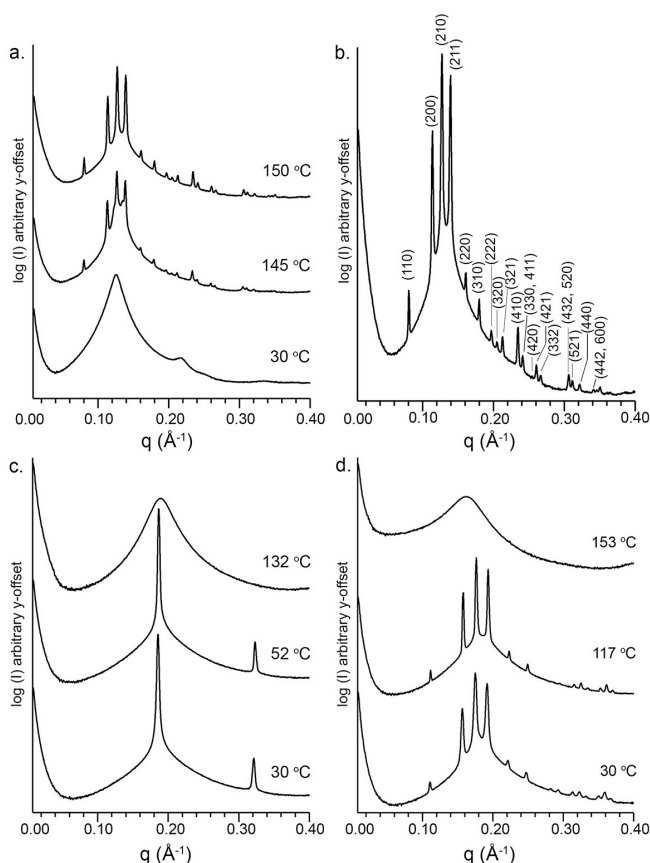
In practice, synthesis of the new aPH domain building blocks was achieved by conducting the living coordination chain transfer polymerization (LCCTP) of 1-hexene according to our previously published methods, which include a reactive quench with molecular iodine (I_2) to provide an intermediate iodo-terminated aPH material that was then converted to the final azido-terminated aPH (**5**) product in standard fashion (see Supporting Information for full details).^[15,20] The desired CB-aPH conjugate **3** was obtained through copper-catalysed click chemistry between **5** and a propargyl-amido-linked CB precursor, while the GAL-aPH conjugate **4**, was produced through a similar click reaction between **5** and a per-acetylated, propargyl ether GAL precursor, followed by standard deprotection of the hydroxyl groups and purification. 1H NMR (800 MHz, $CDCl_3$, 25°C) spectroscopy was used to confirm the identity and purity of **3** and **4**, while size exclusion chromatography (SEC) of **5** and matrix-assisted laser desorption/ionization time-of-flight (MALDI-TOF) mass spectrometry characterization of both **3** and **4** provided data that established the molar mass indices for two different synthetic batches, and more specifically, for **3a** and **4a**, $DP_n=12$, $M_n=1$ kDa, $\bar{D}=1.02$, while for **3b** and **4b**, $DP_n=6$, $M_n=500$ Da, $\bar{D}=1.04$ (see Supporting Information for details).

Synchrotron VT SAXS data were obtained for 1-mm-thick (bulk) samples of each of the **a** and **b** variants of **3** and **4**. Significantly, as Table 1 and Figure 4 confirm, replacement of the aPMP fragment of **1a** with an aPH domain of similar molar mass in the case of **3a** ($DP_n=12$) proved to be a suitable substitute for obtaining a highly ordered A15 mesophase that is observed at 150°C. As Figure 4b shows, the twenty-one Bragg scattering peaks ($q^*=0.0804\text{ Å}^{-1}$) obtained at this temperature were successfully indexed to *hkl* Miller planes with q/q^* values expected for a cubic A15 structure with a unit cell parameter, $a_{A15}=11.05$ nm. In comparison, the thermotropic A15 phase of **1a** was previously reported to have $a_{A15}=10.88$ nm at 180°C.^[15c] First-order estimates for the corresponding spherical particle diameter and volume for **3a** at 150°C are: $d_{\text{sphere}}=6.85$ nm; $V_{\text{sphere}}=168\text{ nm}^3$, while those for **1a** at 180°C are: $d_{\text{sphere}}=6.75$ nm; $V_{\text{sphere}}=161\text{ nm}^3$. This observed 5% increase in V_{sphere} for **3a** over **1a** is seen as supporting evidence for the conclusion that the aPH domain of the former does have a

Table 1: Lattice parameters for A15 and σ mesophases of pure and alloyed blends of **1–4**, including with vitamin E.

Material or Blend	a_{A15} [nm]	a_{σ}, c_{σ} [nm]	Temp. ^[a] [°C]
1a ^[15c]	10.88		180
1b (1 % vit. E) ^[15d]	10.83	10.79, 20.65	210 ^[b]
2a	7.96		117
2b	7.90		101
2b (1 % vit. E)	7.88		60
2b (3 % vit. E)	7.82		56
2b (5 % vit. E)	7.77		47
3a	11.05		150
4b (10 % vit. E)	7.99		30 ^[c]
4b (20 % vit. E)	8.03		30 ^[c]
4b (30 % vit. E)	8.18		30 ^[c]
4b (20 % vit. E)	7.78		117
2:1 1b : 2a	9.41		176
1:1 1b : 2a	9.49		103
1:2 1b : 2b	9.13		97
1:3 1b : 2a	8.84	8.77, 16.69	100, 158
1:4 1b : 2b	8.65		80
1:2 1b : 2b (10 % vit. E)	8.91	8.94, 16.89	102, 127

[a] Temperatures at which lattice parameters were determined, with two temperatures signifying A15 followed by σ . [b] Triple coexistence with A15, σ , and BCC (see Figure 3). [c] Unannealed.

**Figure 4.** Selected synchrotron variable temperature 2D-circularly averaged 1D profile SAXS data for: (a) **3a**, (b) the data in (a) at 150 °C that is indexed to an A15 mesophase, (c) **4b**, and (d) a blend of **4b** with 20% vitamin E.

slightly greater lateral expansion at a lower temperature than the aPMP domain of the latter. It is also important to note that the complete VT SAXS data for **3a** only shows evidence for a H_c morphology, with the distance between cylinders at 30 °C, $d_c = 5.82$ nm, prior to the A15 phase appearing, which then remains highly ordered up to the temperature limit of the experiment at 200 °C (see Figure S16). In contrast, the VT SAXS data for **3b** ($DP_n = 6$), which carries a much shorter aPH tail than **3a**, revealed only formation of a H_c mesophase above 100 °C and up to 200 °C, with the distance between cylindrical domains at 130 °C being $d_c = 4.01$ nm (see Figure S17). Finally, as opposed to success in obtaining an A15 mesophase with **3a**, the VT SAXS data for the GAL-aPH polyolefin conjugate **4a** surprisingly revealed formation of only a BCC mesophase between the entire temperature range of 30 °C to 200 °C, with the calculated lattice and micelle parameters for the SAXS data obtained at 140 °C being: $a_{BCC} = 5.37$ nm; $d_{sphere} = 5.29$ nm; $V_{sphere} = 77$ nm³ (see Figure S18). A similar VT SAXS investigation of **4b** on the other hand showed that a H_c mesophase that spontaneously forms at 30 °C (unannealed), remains the only mesophase, with $d_c = 3.91$ nm at 110 °C, up to reaching a disordered (DIS) state at 132 °C (see Figure 4c). By now turning to the use of blends of **4b** and vitamin E, the desired goal of spontaneously producing a thermotropic sugar-polyolefin conjugate A15 phase at ambient temperature was achieved. More specifically, as Figure 4d and Table 1 reveal, in the absence of any prior thermal annealing, blends consisting of 10 %, 20 %, and 30 % by weight of vitamin E with **4b** resulted in the appearance of highly ordered A15 mesophases in each case, and with a_{A15} increasing as a function of the content of the small molecule phase modulator [cf, $a_{A15} = 7.99$ nm (10 % vitamin E) vs. 8.03 (20 %) vs. 8.18 (30 %) in Table 1]. These ambient temperature A15 mesophases, which are certainly a first for glycolipids, additionally proved to be robust for long periods of time (months) under dry ambient conditions, and as exemplified by the case of **4b** blended with 20 % vitamin E, they are very stable to thermal cycling above the order-disorder transition temperature (e.g. > 153 °C in Figure 4d). Finally, from an indexing of the A15 mesophase for this last blend observed at 117 °C, the unit cell length and estimated spherical micelle parameters were determined to be: $a_{A15} = 7.78$ nm, $d_{sphere} = 4.83$ nm, and $V_{sphere} = 59$ nm³, respectively. This last value corresponds to a remarkable 63 % decrease in volume relative to that estimated for idealized spherical micelle particles for the A15 mesophase of either **1a** or **3a**.

Success in obtaining a stable A15 mesophase for blends of the GAL-aPH conjugate **4b** with vitamin E gave us reason to reinvestigate more carefully the thermotropic phase behaviour of the GAL-aPMP conjugate **2** that we had previously reported.^[15a] Accordingly, new synthetic batches of this sugar-polyolefin conjugate were produced by the reported methods, and these were characterized as having the molar mass indices for **2a** ($DP_n = 8$) and **2b** ($DP_n = 7$) with $D = 1.03$ (see Figure 2). Most significantly, synchrotron VT-SAXS studies of 1-mm-thick bulk samples revealed that both **2a** and **2b** do indeed rapidly produce a thermotropic A15 mesophase above 60 °C, and structural analysis of the

data for **2a** at 117 °C provided the parameters: $a_{A15} = 7.96$ nm, $d_{\text{sphere}} = 4.99$ and $V_{\text{sphere}} = 65$ nm³. Similar structural values were also obtained for the A15 mesophase of **2b** (cf. $a_{A15} = 7.90$ nm at 101 °C), however, a side-by-side comparison of the stacked VT-SAXS data for the two samples of **2** also revealed subtle differences in phase behaviour that are most likely the result of the small change in DP_n values (see Figure S25). Finally, Table 1 also presents results obtained for a study of the phase behaviour of blends of **2b** with increasing amounts of vitamin E that was conducted with the hope of new FK mesophases emerging. As revealed, however, only the appearance of an A15 occurred with 1 %, 3 % and 5 % blends, along with a lowering of the onset temperature for this mesophase as the content of vitamin E increased.

The collective synchrotron SAXS results obtained for both the disaccharide- and monosaccharide-aPMP conjugates **1** and **2**, respectively, established that stable thermotropic A15 mesophases could be obtained with substantially different unit cell parameters and micelle particle size – and in the absence of vitamin E. This new capability next raised the intriguing question presented in Figure 5 of whether “alloys” consisting of blends of two distinctly different FK-mesophase-forming sugar-polyolefin conjugates, such those represented by **1** and **2**, can give rise to the formation of new *chimeric* thermotropic A15 mesophases via the TCP-packing of two different micelle size populations. In this regard, Cheng and co-workers^[11] have successfully pioneered the use of “giant” molecular amphiphiles with constrained spatial geometries to access thermotropic QC and FK mesophases, and through a similar chimeric, or Lego[®]-inspired, building block approach, these investigators have been able to extend the range of TCP-based mesophases even further. Figure 5 also presents an alternative outcome of alloying different sugar-polyolefin conjugates, and namely, the possible formation of “hybrid” A15 mesophases from the TCP-packing of a population of micelle particles with an “averaged” set of dimensional parameters that emerge as a sum of contributions made by both glycolipid components.^[21] This unique alternative hybrid structural model, if validated, might permit the programmed tunability of the A15 lattice parameter by simply changing the alloying ratio of the two types of sugar-polyolefins building blocks – a feat that has not been previously achieved for any soft material FK mesophases.

Table 1 further presents a summary of the results obtained for thermotropic FK mesophases that were

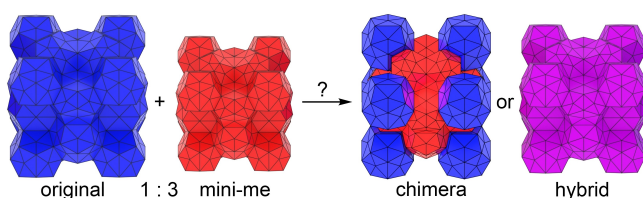


Figure 5. Schematic representations of different possible outcomes for thermotropic A15 mesophases derived from “alloys” of two different FK-phase-forming sugar-polyolefin conjugates.

produced and structurally characterized by synchrotron VT SAXS for a series of alloy blends of **1** and **2** in different ratios. Significantly, as can be seen, these data established a clear trend of decreasing a_{15} lattice parameter for the series of observed A15 mesophases with an increase in the content of the monosaccharide-aPMP **2** over that of the disaccharide-aPMP **1**. Curiously, however, only the 1:3 alloy blend of **1b** : **2a** provided evidence for other TCP-based phases, with a σ mesophase having emerged at 158 °C during the initial temperature ramp conducted at 0.2 °C min^{−1}. Isothermal annealing of this 1:3 alloy at 140 °C for 6.6 h then provided a pure σ mesophase as confirmed by SAXS analysis, and for which values of the lattice parameters, $a_{\sigma} = 8.77$ nm and $c_{\sigma} = 16.69$ nm ($c_{\sigma}/a_{\sigma} = 1.90$ and $c_{\sigma(158^{\circ}\text{C})}/a_{A15(100^{\circ}\text{C})} = 1.89$), could be determined (see Supporting Information). Unfortunately, attempts to directly observe an A15 \rightarrow σ order-order phase transition for this 1:3 **1b** : **2a** blend gave unsatisfactory results. On the other hand, a repeat of this study employing a 1:3 alloy of **1b** : **2b** now provided evidence of a potential DDQC mesophase appearing at 83 °C that then transformed upon heating into an A15 at 91 °C before reaching DIS at 138 °C, but without a σ mesophase having ever emerged.

Prior success with being able to manipulate the thermotropic phase behaviour of sugar-polyolefin conjugates more extensively by blending with vitamin E prompted us to employ this strategy with alloys of the CB-aPMP and GAL-aPMP conjugates, **1** and **2**, respectively, as well. Gratifyingly, after some additional surveying of different blends, the synchrotron VT-SAXS data obtained for a 1:2 alloy of **1b** : **2b** blended with varying amounts of vitamin E finally delivered the equivalent of a “Rosetta Stone” that could be used to decipher the unique thermotropic phase behaviour of these glycolipids, and by extension, potentially for the broader class of all soft materials.

Figure 6 presents partial synchrotron VT SAXS data obtained for the 1:2 alloy of **1b** : **2b** with 10 % vitamin E starting at an initial temperature of 30 °C (unannealed) and increasing to 200 °C with a thermal ramp of 0.2 °C min^{−1}, which corresponds to a time interval between data acquisitions of $\Delta t = 147$ s. Remarkably, one can see a smooth progression of transitions between several phases for this single material in the order: LLP \rightarrow DDQC \rightarrow A15 \rightarrow σ \rightarrow DIS. The LLP to DDQC phase transition closely resembles similar reported observations with other categories of soft materials, however, in the present study, we have been able to capture the kinetics of this transformation on a much shorter timeframe of only seconds. Of particular note is the emergence of the (00002) Bragg reflection for the DDQC mesophase at $q = 0.1395$ Å^{−1}, which corresponds to a periodic z -stacking parameter for the 2D square-triangle tiling planes (see Figure 1c) of $c_{\text{DDQC}} = 9.02$ nm. The successful further indexing of the 10 Bragg reflections of the pure DDQC mesophase that appears at 88.7 °C, as shown in Figure 6c, also provided a value of the square-triangle edge-length parameter, $a_{\text{DDQC}} = 8.86$ nm (see Supporting Information for details). Above this temperature, the series of stacked 2D-circularly averaged 1D SAXS profiles also clearly establish the emergence of A15 from DDQC, and initially in the absence of the σ mesophase. Figure 6b then

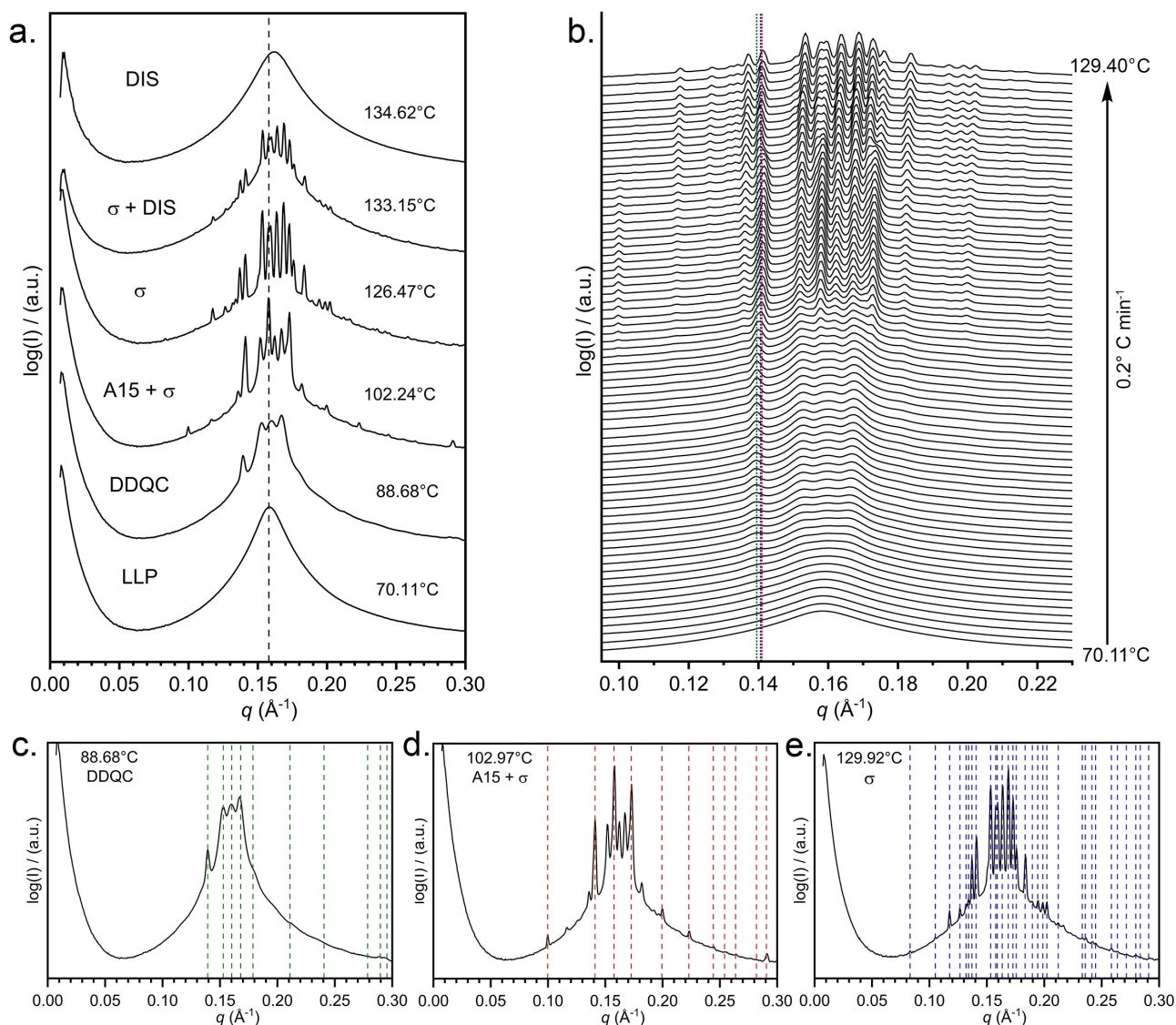


Figure 6. Synchrotron VT SAXS analysis of a 1 : 2 alloy of **1b** : **2b** blended with 10% vitamin E providing: (a) selected 1D profiles of 2D-circularly averaged SAXS data for a temperature ramp from 30 °C to 200 °C at 0.2 °C min⁻¹ that revealed emergence of mesophases in the order of increasing temperature as: LLP < DDQC < A15 < σ < DIS (the black dashed line is for $q = 0.158 \text{ \AA}^{-1}$ centered on the peak maximum of LLP), (b) stacked plot of all 1D SAXS profiles acquired between 70.11 °C and 129.40 °C with a temperature ramp as in (a) and an interval time between data acquisition of 147 s [green dotted line corresponds to the (00002) Bragg reflection ($q = 0.1395 \text{ \AA}^{-1}$) of DDQC, red dotted line corresponds to the (200) Bragg reflection ($q = 0.1410 \text{ \AA}^{-1}$) of A15, and blue dotted line corresponds to the (002) Bragg reflection ($q = 0.1407 \text{ \AA}^{-1}$) of σ], (c) 1D SAXS profile with selected Bragg reflections (green dashed lines) indexed to a DDQC mesophase to provide the parameters, $a_{\text{DDQC}} = 8.86 \text{ nm}$ and $c_{\text{DDQC}} = 9.02 \text{ nm}$, which correspond to the edge length within the xy plane and the periodic stacking in the z direction, respectively, of the triangle-square tiling scheme of Figure 1c, (d) 1D SAXS profile of an A15 + σ mixture with selected Bragg reflections (red dashed lines) indexed to A15 to provide the parameter, $a_{\text{A15}} = 8.91 \text{ nm}$, (e) 1D SAXS profile with selected Bragg reflections (blue dashed lines) indexed to a σ mesophase to provide the parameters, $a_{\sigma} = 8.94$ and $c_{\sigma} = 16.89$ ($c_{\sigma}/a_{\sigma} = 1.89$).

reveals that as temperature continues to increase, the A15 mesophase is cleanly and rapidly converted into σ, until at 127 °C, only the pure σ mesophase exists. Successful indexing of the Bragg reflections to both the A15 and σ lattices that are shown in Figures 6d and 6e, respectively, provide the following unit cell parameters and ratios: $a_{\text{A15}(103^{\circ}\text{C})} = 8.91 \text{ nm}$ and $a_{\sigma(127^{\circ}\text{C})} = 8.94 \text{ nm}$, $c_{\sigma(127^{\circ}\text{C})} = 16.89 \text{ nm}$, respectively, with $c_{\sigma} / a_{\sigma} = 1.89$ and $c_{\sigma(127^{\circ}\text{C})}/a_{\text{A15}(103^{\circ}\text{C})} = 1.90$. The extremely close values observed for the periodic lattice parameters for all three mesophases, [DDQC, A15, and σ], is also striking

and highlighted further with the near unity ratios that exist between several pairs (cf. $c_{\text{DDQC}(89^{\circ}\text{C})}/a_{\text{A15}(103^{\circ}\text{C})} = 1.01$; $c_{\text{DDQC}(89^{\circ}\text{C})}/a_{\sigma(127^{\circ}\text{C})} = 1.00$ and $a_{\sigma(127^{\circ}\text{C})}/a_{\text{A15}(103^{\circ}\text{C})} = 1.00$). Finally, Figure 7 presents results that were obtained from a multi-component regression (MCR) analysis of the entire VT SAXS data set of Figure 6 that served to quantify the relative amounts of the contributing mesophases that exist at each temperature.^[22] Here the Δ5.65 °C gap that appears between 119 °C and 124 °C is due to an unplanned experimental halt in data acquisition that occurred.

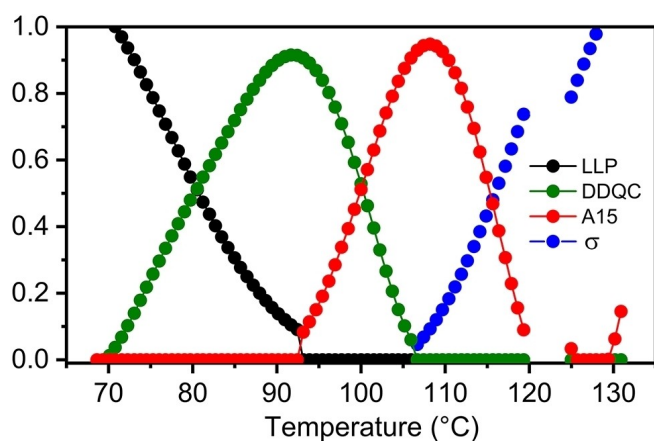


Figure 7. Results of a MCR analysis of the total data set of 1D VT SAXS profiles of Figure 6 with plots of mesophase composition as function of temperature. The $\Delta 5.65^\circ\text{C}$ gap between 119°C and 124°C is due to a halt in data collection.

It is clear from the results presented in Figures 6 and 7 that the phase transitions for the 1:2 alloy of **1b** : **2b** blended with 10 % vitamin E occur sequentially in discrete steps according to $\text{LLP} \rightarrow \text{DDQC}$, followed by $\text{DDQC} \rightarrow \text{A15}$, and then $\text{A15} \rightarrow \sigma$. The near unity ratios between the periodic parameters for DDQC, A15, and σ , and the very short timeframes in which all phase transitions occur, are very supportive of diffusionless martensitic processes. Thus, despite the large apparent difference in unit cell complexity, these results indicate that there must exist a low energy barrier pathway for converting the A15 lattice (with 8 particles per unit cell) into the σ lattice (with 30 particles per unit cell) through an order-order phase transition that proceeds with a minimal change in the dimensions of the participating micelles, in agreement with our previous report and hypothesis (see Figure 3).^[15d] We further posit that these new data and observations are incongruent with a phase transition mechanism that proceeds for the bulk material through a reconstructive diffusive process involving inter-micellar mass transfer, micelle-size self-sorting, and TCP repacking.

Figures 8 and 9 present the foundations for understanding both the mechanism and driving force associated with the $\text{A15} \rightarrow \sigma$ order-order phase transition observed in the present study. To begin, as first proposed by Ishimasa and Fukano^[23] to account for a similar phase transition observed within bimetallic Ni–Cr alloys, this $\text{A15} \rightarrow \sigma$ phase transition can proceed through introduction of two planar defects in both the (100) and (010) planes of an initial A15 lattice to directly provide the final σ unit cell. Notably, the $c_\sigma/a_{\sigma(\text{A15})}$ ratio of 2 that is predicted for the “hard sphere” bimetallic alloy is slightly larger than the corresponding c_σ/a_σ values of between 1.89 and 1.90 that have been reported to date for soft matter FK σ mesophases. It is reasonable to conclude that this difference is a manifestation of the ability of the deformable micelles of soft materials to reshape and space fill the associated WS polyhedra of the σ mesophase more compactly. It is also important to note that Cheng and co-

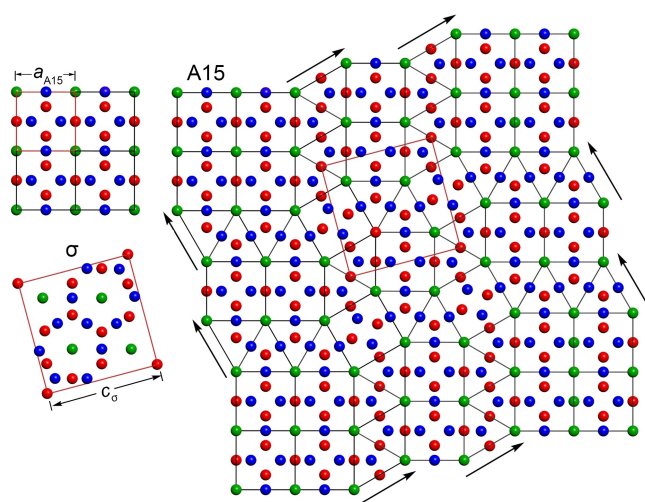


Figure 8. Proposed martensitic $\text{A15} \rightarrow \sigma$ phase transition proceeding through introduction of two planar defects in the (100) and (010) planes of an initial A15 lattice.^[23]

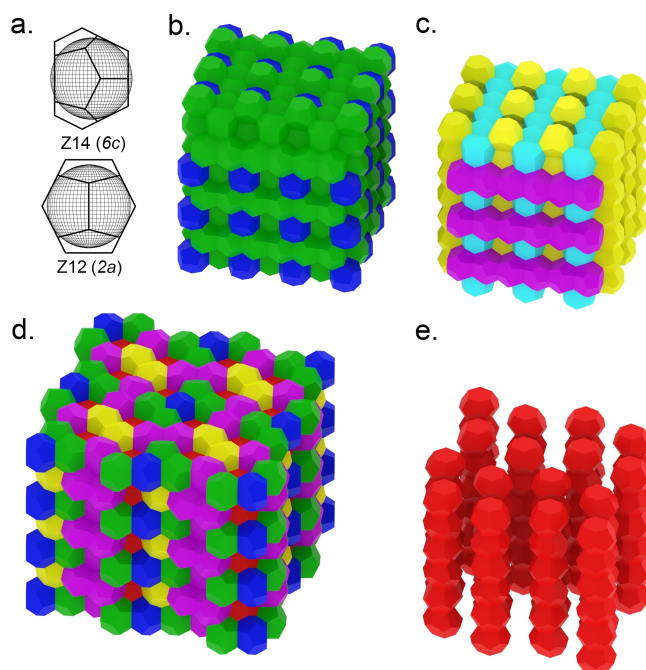


Figure 9. (a) 2D projections of the Z12 (2a) and Z14 (6c) polyhedra of A15 enclosing a sphere that just fits within the former, (b) extended A15 lattice showing unit cell packing according to Figure 1, (c) same lattice as in (b) showing only the three orthogonal hexagon-face-sharing stacks of Z14 polyhedra, (d) extended σ lattice showing unit cell packing according to Figure 1, and (e) same lattice of (d) showing only the single type of hexagon-face-sharing stacks of corresponding Z14 polyhedra.

workers^[11] have obtained experimental evidence for a thermotropic $\text{A15} \rightarrow \text{Z}$ order-order phase transition in their seminal discovery of a soft matter FK Z mesophase for giant shape-constrained amphiphiles. These investigators similarly adopted a mechanism that was previously proposed for a $\text{A15} \rightarrow \text{Z}$ order-order phase transition observed in bimetallic

alloys that proceeds through introduction of two planar defects into only the (100) plane of the A15 lattice to directly provide the Z lattice.^[24,25] It is also of interest that SAXS investigations have been reported for other diffusionless martensitic phase transitions between block copolymer micelle mesophases, including ones involving the introduction of stack faults.^[26]

The remaining questions for the proposed thermotropic martensitic A15 $\rightarrow\sigma$ phase transition of Figure 8 then become, what is the driving force behind this transformation, and can an answer provide new insights for reliably predicting the relative stabilities of other canonical and noncanonical thermotropic soft matter mesophases and the mechanistic nature of order-order phase transitions connecting them? To begin, we note that A15 is also famously known as the Weaire-Phelan (WP) structure in the capacity of it providing a better 3D geometric solution than that proposed by Lord Kelvin for dividing an idealized foam of equal-sized bubbles into equal volume cells of minimum surface area.^[27] Extension of the fundamental principles and geometric analyses upon which the WP solution is based have provided foundational support for subsequent efforts to elucidate the entropic and enthalpic factors that govern the relative stabilities of the broader class of TCP-based structures comprised of deformable core-corona micelles of soft materials, and most notably, those of dendritic liquid crystals and block copolymers.^[1,28] This body of work has further led to the introduction of several physical concepts and parameters associated with the different WS polyhedra shapes and sizes, such as those for tracking the magnitude of chain-packing frustration, τ , and degree of sphericity, ξ . Figure 9 summarizes some of these considerations that are useful for qualitatively assessing the relative stabilities of the A15 vs σ mesophases of sugar-polyolefin conjugates and the origin of the driving force behind the observed A15 $\rightarrow\sigma$ order-order phase transition in the present report. Thus, according to a proposal first presented by Percec, Ungar and co-workers,^[6b,d] it is clear from a comparison of the Z12 and Z14 WS polyhedra of A15, that the former has a lower degree of corona chain packing frustration due to a higher degree of sphericity, while in the latter, corona chains get compressed at the two opposing hexagonal faces, but then need to substantially elongate to fill in the void volume near the vertices. Figures 9b and 9c further show that an extended A15 lattice has three sets of orthogonally oriented columns of these Z14 polyhedra that are stacked through hexagonal face-sharing. In contrast, an extended lattice model of the σ mesophase possesses only a single set of hexagonal face-sharing stacked columns of Z14 polyhedra (see Figures 9d and 9e). Thus, as temperature increases, one can see that the A15 lattice should become more destabilized than that of the σ mesophase due to an increase in chain packing pressure that occurs predominantly at the shared hexagonal faces. It is proposed that this increased pressure on the A15 lattice then leads to introduction of strain-induced planar defects leading to the σ lattice (see Figure 8). Using a similar qualitative argument, it follows that further destabilization of the σ mesophase should occur in favour of a BCC lattice in which no Z14 polyhedra stacking now exists. Swelling of

the WS polyhedra and destabilization of Z14 columnar stacking through incorporation of vitamin E into the corona hydrophobic domains should also result in the same order of increasing appearance of A15 $\rightarrow\sigma$ \rightarrow BCC as percent content of the small molecule modulator increases (see Figure 3). Finally, although not yet considered in any reported modelling of relative TCP-mesophase stability, we believe that, for thermotropic phases, the large role that van der Waal attractive interactions between the corona of face sharing WS polyhedra can play in stabilizing one mesophase over the other has largely not been adequately accounted for. Accordingly, we further posit that the sequence of LLP initially organizing into DDQC, which then transforms into A15 as a function of increasing temperature, is largely initially directed and dictated by attractive and stabilizing van der Waal interactions between Z14 hexagonal face sharing – up to the limit of temperature-induced chain dynamics that now destabilize this face-sharing interaction. A more quantitative assessment of how one might be able to control this fine balance of opposing factors for polyhedra face-sharing could lead to new soft matter TCP-based mesophases on demand rather than through serendipity.

Conclusion

The present report serves to significantly expand the foundations of the thermotropic supramolecular organization of glycolipids by employing readily available and structurally versatile sugar-polyolefin conjugates. In addition to providing the first example of a glycolipid dodecagonal quasicrystal and demonstration that both DDQC and FK A15 mesophases can be produced at ambient temperature, observation of the first direct rapid A15 $\rightarrow\sigma$ order-order phase transition is documented. Importantly, the mechanism of this transformation can be rationalized as proceeding through a well-established martensitic process involving introduction of strain-induced planar defects into the initial A15 lattice. Qualitative consideration of the driving force dictating the relative stabilities of A15, σ and BCC lattices provides an intuitive strategy that can be used to design and obtain other thermotropic TCP-based mesophases in programmed fashion. The inclusion and importance of corona-corona van der Waal interactions that occur for polygon face sharing between adjacent WS polyhedra should be included to predict the relative stabilities of various QC and FK mesophases more accurately. Finally, given the demonstrated relative ease with which glycolipid thermotropic QC and FK mesophases can now form, there is a high probability that naturally occurring analogues can be found to exist under the conditions of terrestrial and non-terrestrial environments.

Author Contributions

C.M.W. and K.K.L. are recognized as first co-authors and equally contributed to the synthesis and analytical and spectroscopic characterization, as well as VT SAXS, of all

new sugar-polyolefin conjugates, including blends with vitamin E. Synchrotron VT SAXS investigations were aided by E.H.R.T, who also performed the MCR analysis. L.R.S. supervised the project, wrote the manuscript, and created most data and all non-data figures and schemes. All authors contributed to the analysis and figures of VT SAXS data that are presented, and, in the review and revision of the final manuscript.

Experimental Section

Experimental details are provided in the Supporting Information.

Acknowledgements

This research used resources of the Center for Functional Nanomaterials and the National Synchrotron Light Source II, which are U.S. DOE Office of Science Facilities, at Brookhaven National Laboratory under Contract No. DESC0012704. We thank the National Science Foundation for support for the acquisition of SAXS and AFM instruments (DMR-1228957 and MRI 1626288, respectively) and a high field 800 MHz NMR spectrometer (BDI-1040158). Support of this work was provided by a grant from the National Science Foundation (NSF) (CHE-1955730) to L.R.S for which he is grateful. We also wish to thank Dr. Kevin Yager of BNL for fruitful discussions and Prof. Sangwoo Lee (Rensselaer) for sharing coordinates of the WS polyhedra for A15 and σ phases.

Conflict of Interest

The corresponding author has a financial interest in the university spin-out company, Precision Polyolefins, LLC (PPL). This work did not involve any PPL personnel, funding, or other resources and all new intellectual property has been disclosed in accordance with state and federal requirements.

Data Availability Statement

The data that support the findings of this study are available from the corresponding author upon reasonable request.

Keywords: Frank–Kasper • Glycolipid • Mesophase • Quasicrystal

- [1] For some reviews and perspectives, see: a) G. Ungar, X. Zeng, *Soft Matter* **2005**, *1*, 95–106; b) G. Ungar, V. Percec, X. Zeng, P. Leowanawat, *Isr. J. Chem.* **2011**, *51*, 1206–1215; c) M. Huang, K. Yue, J. Wang, C.-H. Hsu, L. Wang, S. Z. D. Cheng, *Sci. China Chem.* **2018**, *61*, 33–45; d) K. D. Dorfman, *Macromolecules* **2021**, *54*, 10251–10270; e) V. Percec, D. Sahoo, *Giant* **2022**, *12*, 100127.

- [2] a) G. Ashkenasy, T. M. Hermans, S. Otto, A. F. Taylor, *Chem. Soc. Rev.* **2017**, *46*, 2543–2554; b) A. F. Mason, N. A. Yewdall, P. L. W. Welzen, J. Shao, M. van Stevendaal, J. C. M. van Hest, D. S. Williams, L. K. E. A. Abelmohsen, *ACS Cent. Sci.* **2019**, *5*, 1360–1365; c) V. Percec, Q. Xiao, *Isr. J. Chem.* **2021**, *61*, 530–556.
- [3] a) N. Chandrasekhar, R. Chandrasekar, *Angew. Chem. Int. Ed.* **2012**, *51*, 3556–3561; b) L.-L. Ma, C.-Y. Li, J.-T. Pan, Y.-E. Ji, C. Jiang, R. Zheng, Z.-Y. Wang, B.-X. Li, Y.-Q. Lu, *Light: Sci. Appl.* **2022**, *11*, 270; c) D.-Y. Guo, C.-W. Chen, C.-C. Li, H.-C. Jau, K.-H. Lin, T.-M. Feng, C.-T. Wang, T. J. Bunning, I. C. Khoo, T.-H. Lin, *Nat. Mater.* **2020**, *19*, 94–101; d) J. Liu, W. Liu, B. Guan, B. Wang, L. Shi, F. Jin, Z. Zheng, J. Wang, T. Ikeda, L. Jiang, *Nat. Commun.* **2021**, *12*, 3477.
- [4] a) F. C. Frank, J. S. Kasper, *Acta Crystallogr.* **1958**, *11*, 184–190; b) F. C. Frank, J. S. Kasper, *Acta Crystallogr.* **1959**, *12*, 483–499.
- [5] a) X. Zeng, G. Ungar, *Philos. Mag.* **2006**, *86*, 1093–1103; b) R. Lifshitz, H. Diamant, *Philos. Mag.* **2007**, *87*, 3021–3030.
- [6] a) V. S. K. Balagurusamy, G. Ungar, V. Percec, G. Johansson, *J. Am. Chem. Soc.* **1997**, *119*, 1539–1555; b) S. D. Hudson, H.-T. Jung, V. Percec, W.-D. Cho, G. Johansson, G. Ungar, V. S. K. Balagurusamy, *Science* **1997**, *278*, 449–452; c) V. Percec, C.-H. Ahn, G. Ungar, D. J. P. Yearley, M. Möller, S. S. Sheiko, *Nature* **1998**, *391*, 161–164; d) G. Ungar, Y. Liu, X. Zeng, V. Percec, W.-D. Cho, *Science* **2003**, *299*, 1208–1211; e) X. B. Zeng, G. Ungar, Y. S. Liu, V. Percec, S. E. Dulcey, J. K. Hobbs, *Nature* **2004**, *428*, 157–160; f) V. Percec, M. R. Imam, M. Peterca, D. A. Wilson, R. Graf, H. W. Spiess, V. S. K. Balagurusamy, P. A. Heiney, *J. Am. Chem. Soc.* **2009**, *131*, 7662–7677; g) B. M. Rosen, D. A. Wilson, C. J. Wilson, M. Peterca, B. C. Won, C. Huang, L. R. Lipski, X. Zeng, G. Ungar, P. A. Heiney, V. Percec, *J. Am. Chem. Soc.* **2009**, *131*, 17500–17521; h) M. Peterca, M. R. Imam, P. Leowanawat, B. M. Rosen, D. A. Wilson, C. J. Wilson, X. Zeng, G. Ungar, P. A. Heiney, V. Percec, *J. Am. Chem. Soc.* **2010**, *132*, 11288–11305; i) M. N. Holerca, D. Sahoo, M. Peterca, B. E. Partridge, P. A. Heiney, V. Percec, *Macromolecules* **2017**, *50*, 375–385; j) M. N. Holerca, D. Sahoo, B. E. Partridge, M. Peterca, X. Zeng, G. Ungar, V. Percec, *J. Am. Chem. Soc.* **2018**, *140*, 16941–16947; k) D. A. Wilson, K. A. Andreopoulos, M. Peterca, P. Leowanawat, D. Sahoo, B. E. Partridge, Q. Xiao, N. Huang, P. A. Heiney, V. Percec, *J. Am. Chem. Soc.* **2019**, *141*, 6162–6166; l) V. Percec, N. Huang, Q. Xiao, B. E. Partridge, D. Sahoo, M. R. Imam, M. Peterca, R. Graf, H.-W. Spiess, X. Zeng, G. Ungar, *Giant* **2022**, *9*, 100084.
- [7] a) K. Borisch, S. Diele, P. Göring, C. Tschierske, *Chem. Commun.* **1996**, 237–238; b) K. Borisch, S. Diele, P. Göring, H. Kresse, C. Tschierske, *Angew. Chem. Int. Ed. Engl.* **1997**, *36*, 2087–2089; c) K. Borisch, C. Tschierske, P. Göring, S. Diele, *Chem. Commun.* **1998**, 2711–2712; d) K. Borisch, S. Diele, P. Göring, H. Mglle, C. Tschierske, *Liq. Cryst.* **1997**, *22*, 427–443; e) K. Borisch, S. Diele, P. Göring, H. Kresse, C. Tschierske, *J. Mater. Chem.* **1998**, *8*, 529–543; f) H. Dai, X. Yang, X. Tan, F. Su, X. Cheng, F. Liu, C. Tschierske, *Chem. Commun.* **2013**, 49, 10617–10619.
- [8] T. Jun, H. Park, S. Jeon, S. Jo, H. Ahn, W.-D. Jang, B. Lee, D. Y. Ryu, *J. Am. Chem. Soc.* **2021**, *143*, 17548–17556.
- [9] a) S. Lee, M. J. Bluemle, F. S. Bates, *Science* **2010**, *330*, 349–353; b) J. Zhang, F. S. Bates, *J. Am. Chem. Soc.* **2012**, *134*, 7636–7639; c) S. Lee, C. Leighton, F. S. Bates, *Proc. Natl. Acad. Sci. USA* **2014**, *111*, 17723–17731; d) S. Chanpuriya, K. Kim, J. Zhang, S. Lee, A. Arora, K. D. Dorfman, K. T. Delaney, G. H. Fredrickson, F. S. Bates, *ACS Nano* **2016**, *10*, 4961–4972; e) M. W. Schulze, R. M. Lewis III, J. H. Lettow, R. J. Hickey, T. M. Gillard, M. A. Hillmyer, F. S. Bates, *Phys. Rev. Lett.* **2017**, *118*, 207801; f) K. Kim, M. W. Schulze, A.

- Arora, R. M. Lewis III, M. A. Hillmyer, K. D. Dorfman, F. S. Bates, *Science* **2017**, 356, 520–523; g) A. Reddy, M. B. Buckley, A. Arora, F. S. Bates, K. D. Dorfman, G. M. Grason, *Proc. Natl. Acad. Sci. USA* **2018**, 115, 10233–10238; h) A. B. Chang, F. S. Bates, *ACS Nano* **2020**, 14, 11463–11472; i) A. J. Mueller, A. P. Lindsay, A. Jayarama, T. P. Lodge, M. K. Mahanthappa, F. S. Bates, *Macromolecules* **2021**, 54, 2647–2660; j) A. P. Lindsay, G. K. Cheong, A. J. Peterson, S. Weigand, K. D. Dorfman, T. P. Lodge, F. S. Bates, *Macromolecules* **2021**, 54, 7088–7101; k) A. J. Mueller, A. P. Lindsay, A. Jayarama, S. Weigand, T. P. Lodge, M. K. Mahanthappa, F. S. Bates, *Macromolecules* **2022**, 55, 8332–8344.
- [10] a) K. Hayashida, T. Dotera, A. Takano, Y. Matsushita, *Phys. Rev. Lett.* **2007**, 98, 195502; b) H. Y. Jung, M. J. Park, *Soft Matter* **2017**, 13, 250–257; c) H. Takagi, R. Hashimoto, N. Igarashi, S. Kishimoto, K. Yamamoto, *J. Phys. Condens. Matter* **2017**, 29, 204002; d) H. Takagi, K. Yamamoto, *Macromolecules* **2019**, 52, 2007–2014; e) M. W. Bates, J. Lequieu, S. M. Barbon, R. M. Lewis III, K. T. Delaney, A. Anastasaki, C. J. Hawker, G. H. Fredrickson, C. M. Bates, *Proc. Natl. Acad. Sci. USA* **2019**, 116, 13194–13199; f) S. Jeon, T. Jun, S. Jo, H. Ahn, S. Lee, B. Lee, D. Y. Ryu, *Macromol. Rapid Commun.* **2019**, 40, 1900259; g) Y. Sun, R. Tan, Z. Ma, Z. Gan, G. Li, D. Zhou, Y. Shao, W.-B. Zhang, R. Zhang, X.-H. Dong, *ACS Cent. Sci.* **2020**, 6, 1386–1393; h) K. Yamamoto, H. Takagi, *Mater. Trans.* **2021**, 62, 325–328; i) Z. Ma, R. Tan, Z. Gan, D. Zhou, Y. Yang, W. Zhang, X.-H. Dong, *Macromolecules* **2022**, 55, 4331–4340; j) M.-Z. Chen, Y.-T. Huang, C.-Y. Chen, H.-L. Chen, *Macromolecules* **2022**, 55, 10812–10820.
- [11] a) M. Huang, C.-H. Hsu, J. Wang, S. Mei, X. Dong, Y. Li, M. Li, H. Liu, W. Zhang, T. Aida, W.-B. Zhang, K. Yue, S. Z. D. Cheng, *Science* **2015**, 348, 424–428; b) K. Yue, M. Huang, R. L. Marson, J. He, J. Huang, Z. Zhou, J. Wang, C. Liu, X. Yan, K. Wu, Z. Guo, H. Liu, W. Zhang, P. H. Ni, C. Wesdemiotis, W.-B. Zhang, S. C. Glotzer, S. Z. D. Cheng, *Proc. Natl. Acad. Sci. USA* **2016**, 113, 14195–14200; c) W. Zhang, X. Lu, J. Mao, C.-H. Hsu, G. Mu, M. Huang, Q. Guo, H. Liu, C. Wesdemiotis, T. Li, W.-B. Zhang, Y. Li, S. Z. D. Cheng, *Angew. Chem. Int. Ed.* **2017**, 56, 15014–15019; d) Z. Su, C.-H. Hsu, Z. Gong, X. Feng, J. Huang, R. Zhang, Y. Wang, J. Mao, C. Wesdemiotis, T. Li, S. Seifert, W. Zhang, T. Aida, M. Huang, S. Z. D. Cheng, *Nat. Chem.* **2019**, 11, 899–905; e) Z. Su, J. Huang, W. Shan, X.-Y. Yan, R. Zhang, T. Liu, Y. Liu, Q.-Y. Guo, F. Bian, X. Miao, M. Huang, S. Z. D. Cheng, *CCS Chem.* **2021**, 3, 1434–1444; f) J. Huang, R. Zhang, Y. Wang, Z. Su, X.-Y. Yan, Q.-Y. Guo, T. Liu, Y. Liu, H. Lei, M. Huang, W. Zhang, S. Z. D. Cheng, *Macromolecules* **2021**, 54, 7777–7785; g) X. Y. Yan, Q.-Y. Guo, X.-Y. Liu, Y. Wang, J. Wang, Z. Su, J. Huang, F. Bian, H. Lin, M. Huang, Z. Lin, T. Liu, Y. Liu, S. Z. D. Cheng, *J. Am. Chem. Soc.* **2021**, 143, 21613–21621; h) Y. Wang, J. Huang, X.-Y. Yan, H. Lei, X.-Y. Liu, Q.-Y. Guo, Y. Liu, T. Liu, M. Huang, F. Bian, Z. Su, S. Z. D. Cheng, *Angew. Chem. Int. Ed.* **2022**, 61, e20220637; i) H. Lei, Y. Liu, T. Liu, Q.-Y. Guo, X.-Y. Yan, Y. Wang, W. Zhang, Z. Su, J. Huang, W. Xu, F.-G. Bian, M. Huang, S. Z. D. Cheng, *Angew. Chem. Int. Ed.* **2022**, 61, e202203433; j) Y. Liu, T. Liu, X.-Y. Yan, Q.-Y. Guo, H. Lei, Z. Huang, R. Zhang, Y. Wang, J. Wang, F. Liu, F.-G. Bian, E. W. Meijer, T. Aida, M. Huang, S. Z. D. Cheng, *Proc. Natl. Acad. Sci. USA* **2022**, 119, e215304119.
- [12] S. Fischer, A. Exner, K. Zielske, J. Perlich, S. Deloudi, W. Steurer, P. Lindner, S. Forster, N. A. Clark, *Proc. Natl. Acad. Sci. USA* **2011**, 108, 1810–1814.
- [13] D. Nykypanchuk, M. M. Maye, D. van der Lelie, O. Gang, *Nature* **2008**, 451, 549–552.
- [14] For theoretical investigations of soft matter QC and FK phases relevant to the present report, see: a) C. R. Iacovella, A. S. Keys, S. C. Glotzer, *Proc. Natl. Acad. Sci. USA* **2011**, 108, 20935–20940; b) M. Liu, Y. Qiang, W. Li, F. Qiu, A.-C. Shi, *ACS Macro Lett.* **2016**, 5, 1167–1171; c) A. Arora, J. Qin, D. C. Morse, K. T. Delaney, G. H. Fredrickson, F. S. Bates, K. D. Dorfman, *Macromolecules* **2016**, 49, 4675–4690; d) W. Li, C. Duan, A.-C. Shi, *ACS Macro Lett.* **2017**, 6, 1257–1262; e) K. Kim, A. Arora, R. M. Lewis III, M. Liu, W. Li, A.-C. Shi, K. D. Dorfman, F. S. Bates, *Proc. Natl. Acad. Sci. USA* **2018**, 115, 847–854; f) R. M. Lewis III, A. Arora, H. K. Beech, B. Lee, A. P. Lindsay, T. P. Lodge, K. D. Dorfman, F. S. Bates, *Phys. Rev. Lett.* **2018**, 121, 208002; g) A. P. Lindsay, A. Jayarama, A. J. Peterson, A. J. Mueller, S. Weigand, K. Almdal, M. K. Mahanthappa, T. P. Lodge, F. S. Bates, *ACS Nano* **2021**, 15, 9453–9468; h) D. Li, K. Zhang, *Soft Matter* **2022**, 18, 640–647; i) B. R. Magruder, S. J. Park, R. P. Collanton, F. S. Bates, K. D. Dorfman, *Macromolecules* **2022**, 55, 2991–2998; j) L. J. Case, F. S. Bates, K. D. Dorfman, *Soft Matter* **2023**, 19, 90–97.
- [15] a) T. S. Thomas, W. Hwang, L. R. Sita, *Angew. Chem. Int. Ed.* **2016**, 55, 4683–4687; b) S. R. Nowak, W. Hwang, L. R. Sita, *J. Am. Chem. Soc.* **2017**, 139, 5281–5284; c) K. K. Lachmayr, C. M. Wentz, L. R. Sita, *Angew. Chem. Int. Ed.* **2020**, 59, 1521–1526; d) K. K. Lachmayr, L. R. Sita, *Angew. Chem. Int. Ed.* **2020**, 59, 3563–3567; e) S. R. Nowak, K. K. Lachmayr, K. G. Yager, L. R. Sita, *Angew. Chem. Int. Ed.* **2021**, 60, 8710–8716.
- [16] a) M. Patrick, N. I. Zahid, M. Kriechbaum, R. Hashim, *Liq. Cryst.* **2018**, 45, 1970–1986; b) R. Hashim, N. I. Zahid, T. S. Velayutham, N. F. K. Aripin, S. Ogawa, A. Sugimura, *J. Oleo Sci.* **2018**, 67, 651–668; c) N. A. N. Saari, A. A. Mislán, R. Hashim, N. I. Zahid, *Langmuir* **2018**, 34, 8962–8974.
- [17] a) J. D. Cushen, I. Otsuka, C. M. Bates, S. Halila, S. Fort, C. Rochas, J. A. Easley, E. L. Rausch, A. Thio, R. Borsali, C. G. Willson, C. J. Ellison, *ACS Nano* **2012**, 6, 3424–3433; b) J. D. Cushen, K. Shanmuganathan, D. W. Janes, C. G. Willson, C. J. Ellison, *ACS Macro Lett.* **2014**, 3, 839–844; c) T. Isono, R. Komaki, N. Kawakami, K. Chen, H.-L. Chen, C. Lee, K. Suzuki, B. J. Ree, H. Mamiya, T. Yamamoto, R. Borsali, K. Tajima, T. Satoh, *Biomacromolecules* **2022**, 23, 3978–3989; d) T. Isono, I. Otsuka, Y. Kondo, S. Halila, S. Fort, C. Rochas, T. Satoh, R. Borsali, T. Kakuchi, *Macromolecules* **2013**, 46, 1461–1469; e) K. Aissou, I. Otsuka, C. Rochas, S. Fort, S. Halila, R. Borsali, *Langmuir* **2011**, 27, 4098–4103; f) I. Otsuka, T. Isono, C. Rochas, S. Halila, S. Fort, T. Satoh, T. Kakuchi, R. Borsali, *ACS Macro Lett.* **2012**, 1, 1379–1382; g) T. Isono, S. Nakahira, H.-C. Hsieh, S. Katsuhara, H. Mamiya, T. Yamamoto, W.-C. Chen, R. Borsali, K. Tajima, T. Satoh, *Macromolecules* **2020**, 53, 5408–5417.
- [18] J. W. Goodby, V. Görtz, S. J. Cowling, G. Mackenzie, P. Martin, D. Plusquellec, T. Benvegnu, P. Boullanger, D. Lafont, Y. Queneau, S. Chambert, J. Fitremann, *Chem. Soc. Rev.* **2007**, 36, 1971–2032.
- [19] P. Garidel, Y. Kaonis, L. Heinbockel, M. Wulf, S. Gerber, A. Munk, V. Vill, K. Brandenburg, *Open Biochem. J.* **2015**, 9, 49–72.
- [20] For leading references on LCCTP of olefin see: a) L. R. Sita, *Angew. Chem. Int. Ed.* **2009**, 48, 2464–2472; b) W. Zhang, L. R. Sita, *J. Am. Chem. Soc.* **2008**, 130, 442–443; c) W. Zhang, J. Wei, L. R. Sita, *Macromolecules* **2008**, 41, 7829–7833; d) M. A. Wallace, A. A. Burkey, L. R. Sita, *ACS Catal.* **2021**, 11, 10170–10178; e) A. A. Burkey, D. M. Fischbach, C. M. Wentz, K. L. Beers, L. R. Sita, *ACS Macro Lett.* **2022**, 11, 402–409.
- [21] a) D. Zhao, E. Wang, T. P. Lodge, *Macromolecules* **2020**, 53, 7705–7716; b) S. Kim, S. Lee, S.-H. Choi, K. Char, *Macromolecules* **2021**, 54, 4739–4746.
- [22] X. Qu, D. Yan, R. Li, J. Cen, C. Zhou, W. Zhang, D. Lu, K. Attenkofer, D. J. Stacchiola, M. S. Hybertsen, E. Stavitski, M. Liu, *Chem. Mater.* **2021**, 33, 1740–1751.

- [23] For plane defects in A15, see: a) T. Ishimasa, Y. Fukano, *Jpn. J. Appl. Phys.* **1983**, 22, 1092–1097; b) T. Ishimasa, Y. Fukano, *Surf. Sci.* **1985**, 156, 241–248.
- [24] X. Zhang, J. Zhang, H. Wang, J. Rogal, H.-Y. Li, S.-H. Wei, T. Hickel, *Appl. Phys. Rev.* **2022**, 9, 041311.
- [25] S. Andersson, *J. Solid State Chem.* **1978**, 23, 191–204.
- [26] a) L. Chen, H. S. Lee, M. Zhernenkov, S. Lee, *Macromolecules* **2019**, 52, 6649–6661; b) L.-T. Chen, Y.-T. Huang, C.-Y. Chen, M.-Z. Chen, H.-L. Chen, *Macromolecules* **2021**, 54, 8936–8945.
- [27] D. Weaire, R. Phelan, *Philos. Mag. Lett.* **1994**, 69, 107–110.
- [28] a) P. M. Duesing, R. H. Templer, J. M. Seddon, *Langmuir* **1997**, 13, 351–359; b) R. Gabbrielli, A. J. Meagher, D. Weaire, K. A. Brakke, S. Hutzler, *Philos. Mag. Lett.* **2012**, 92, 1–6; c) M. Rappolt, F. Cacho-Nerin, C. Morello, A. Yaghmur, *Soft Matter* **2013**, 9, 6291–6300.

Manuscript received: February 22, 2023

Accepted manuscript online: April 5, 2023

Version of record online: May 2, 2023